Near-IR absorbing solar cell sensitized with bacterial photosynthetic membranes

Near-IR absorbing solar cell sensitized with bacterial photosynthetic membranes

Kamil Woronowicz[1], Saquib Ahmed[2], Archana A. Biradar[3, 4], Ankush V. Biradar[3, 4], Dunbar P. Birnie, III[2], Tewodros Asefa[3, 4] & Robert A. Niederman[1]

[1]*Department of Molecular Biology and Biochemistry, Rutgers, The State University of New Jersey, 604 Allison Road, Piscataway, NJ 08854-8082, USA*

[2]*Department of Materials Science and Engineering, Rutgers, The State University of New Jersey, 607 Taylor Road, Piscataway, NJ 08854-8065, USA*

[3]*Department of Chemistry and Chemical Biology, Rutgers, The State University of New Jersey, 610 Taylor Road, Piscataway, NJ 08854-8087, USA*

[4]*Department of Chemical and Biochemical Engineering, Rutgers, The State University of New Jersey, 98 Brett Road, Piscataway, NJ 08854- 8058, USA*

In response to the growing worldwide demand for renewable, secure and clean energy sources, a considerable research effort is now being focused on natural photosynthetic processes as a blueprint for solar energy conversion devices.[1,2] This has led to the development of biohybrid photoelectric cells based on natural algal photosynthetic systems[3,4] for the ultimate conversion of sunlight into hydrogen and the generation of electrical currents with algal[5] and plant photosystems[6] as well as near-IR absorbing bacterial photosynthetic membrane vesicles (chromatophores)[7] and their reaction center (RC)[8-11] and RC-light-harvesting 1 (LH1) protein core components.[12] In a recent study, in which chromatophores were adsorbed to a gold electrode surface in conjunction with biological electrolytes (quinone (Q) and cytochrome *c*) as redox mediators, current generation was dependent on an open circuit potential.[6] We therefore tested whether this external potential (-100 mV) could be replaced in an appropriately designed dye-sensitized solar cell (DSSC), capable of generating significant solar-energy driven currents. Here we show that a DSSC system in which the organic light-harvesting dye is replaced by robust chromatophores from *Rhodospirillum rubrum*, in conjunction with Q and cytochrome *c*, represents a major step towards the development a self-contained biosolar cell. This device provides band energies between consecutive interfaces that facilitate a unidirectional flow of electrons. Solar I-V testing demonstrated that it represents a working solar cell, with a relatively high Isc (short-circuit current) of 25 $\mu A/cm^2$, in the absence of an external potential. Importantly, the cell is capable of generating current utilizing abundant near-IR photons (maximum at ~880 nm) with an >8–fold higher energy conversion efficiency than white light. Overall, these studies represent a powerful demonstration of the photoexcitation properties of a biological system in a solid-state device and its successful implementation in a functioning solar cell.

Dye-sensitized solar cells (DSSCs) have come to represent an area of intense research since their inception in 1991[13] as a promising photovoltaic technology owing to their low cost and simplicity of manufacture. A typical DSSC is composed of a mesoporous TiO_2 film, on a transparent conducting fluorine-doped tin oxide (FTO). The TiO_2 layer is coated with a monolayer of sensitizer dye molecules (usually a ruthenium bipyridyl complex), which undergo excitiation upon illumination and inject electrons into the conduction band of the TiO_2 particles. The electrons are channeled to an external circuit to do useful work and re-enter the cell through a Pt-coated counter electrode at the back-contact. A liquid electrolyte generally consisting of an I^-/I_3^- redox couple serves to reduce the photoexcited dye molecules. At the heart of DSSC functionality is the intimate agreement of band energies of the individual consecutive components to ensure electron directionality and flow.

In previous studies of biohybrid solar cells, chromatophores from the purple photosynthetic bacterium *Rhodobacter sphaeroides* have been adsorbed to a gold electrode surface to generate light-dependent currents.[7] These chromatophores contain integral membrane LH proteins that in addition to absorbing blue light, are capable of collecting near-IR photons (800-875 nm) and transferring their excitation energy to the RC bacteriochlorophyll special pair which catalyzes a transmembrane charge separation.[14] This initiates a cycle of electron transfer reactions between the primary iron-quinone acceptor (Q_A), the cytochrome bc_1 complex and cytochrome c_2, accompanied by the formation of an electrochemical proton gradient.

The generation of current by the electrode surface adsorbed *Rba, sphaeroides* chromatophores was dependent on an open circuit potential of -100 mV, providing directionality to the electron flow. Here we have replaced this system with an appropriately designed DSSC, capable of generating a significant solar-energy driven current. Although the *Rba. sphaeroides* LH1

complex, which functions at the interface of light harvesting and electron cycling, was found to be exceptionally stable, the LH2 peripheral antenna showed a light-intensity dependent decoupling from photoconversion.[7] This lack of long-term LH2 stability prompted us to construct a DSSC prototype with chromatophores from the related organism *Rsp. rubrum*, which forms a robust LH1-RC core structure, while lacking LH2.

This chromatophore-sensitized solar cell (CSSC) was assembled using sintered P25 titania, *Rps. rubrum* chromatophores, cytochrome *c* and a ubiquinone analog, lacking an isoprenoid side chain (Q_0) as electrolytes, and was characterized along with control samples lacking one or more of these components. The microstructure of the sintered P25 films used as the photoanode for the CSSC was assessed by mercury porosimetry and field emission scanning electron microscopy (FESEM)(see Supplementary Figs. 1 and 2). Porosimetry demonstrated that cytochrome *c* and Q_0 freely percolate through the P25 TiO_2 matrix, allowing for enhanced charge transfer to take place across the interfaces, while FESEM showed that the chromatophores, which have a diameter of ~50 nm, partially insert into the pores or sit at the surface (see Supplementary Fig. 2).

The results of an extensive solar characterization of CSSCs and the control samples are presented in Table 1 and Figs. 1-2. Rigorous J-V solar characterization under white light showed that as expected, the TiO_2 only cell gave the best performance (Fig. 1A), since TiO_2 has an absorption band edge below 400 nm, harvesting the highest energy photons. The device systems of TiO_2 + cytochrome *c*, TiO_2 + Q_0, or TiO_2 + Q_0 + cytochrome *c* performed less efficiently, since they are incorporating liquid phase electrolytes (equivalents) which closely percolate through the TiO_2 matrix. This opens up recombination centers at the pores, resulting in decreases in both V_{OC} and J_{SC} for these systems in comparison with the TiO_2-only device. Most importantly, these measurements show that the adhered chromatophore (TiO_2 + chromatophores + Q_0 + cytochrome

c) system performs much better than the individual redox mediator-only systems, second only to the TiO_2 device system, thereby demonstrating that light harvesting is indeed occurring as a result of the presence of the chromatophores.

Since the LH1 complex, the major protein of *Rsp. rubrum* chromatophores, has an intense absorbance maximum at 880 nm ($\varepsilon \approx 120\ mM^{-1}cm^{-1}$), the introduction of an 890-nm band pass filter effectively cut off the rest of the light spectrum. Under such conditions, the full CSSC TiO_2 + chromatophores + Q_0 + cytochrome *c* system performed substantially better than any of the controls (Fig. 1B) These results provide definitive proof of not only the light harvesting characteristic of the *in situ* LH1 complex, but also the overall functionality of the CSSC device.

Fig. 2 shows the dark current behavior of the CSSC and control cells, which provides a more complete insight into the recombination kinetics occurring within the TiO_2 matrices. Dark current trends of DSSC films serve as a qualitative measure of the recombination rate of electrons in the TiO_2 conduction band in the presence of electrolyte. A reduction in the recombination rate was indicated by the positive shift in the breakdown voltage during the dark current onset. These data can be used in conjunction with the J-V data to further support dark current trends. The lowest recombination was encountered with the TiO_2-only device system, since no additional components are present where recombination can occur. When compared to the redox mediators alone, the full CSSC (TiO_2 + chromatophores + Q_0 + cytochrome *c*) system showed the least recombination. We can explain this phenomenon by the chromatophores attached at the TiO_2 surface serving as a barrier layer between electrons recombining with the Q_0/cytochrome *c*. When chromatophores were bound to the surface of the working electrode in the presence of electrolytes, the significant reduction in back transfer rate suggests a very good coupling between the biological electrolytes and the electrode, while the unidirectionality of electron flow within

the “biological” dye is in agreement with the band diagram (see below). This also suggests that the chromatophores bind to the TiO_2 surface with the cytosolic face of the RC oriented toward TiO_2. The probability of back transfer of excitation energy in *Rsp. rubrum* chromatophores from the RC to LH1 has been reported to be 25%,[16] providing additional support that the flow of excitation is also unidirectional within the chromatophores.

The energetics and band matching of the various components serve as critical factors in governing the operation of a DSSC device. Fig. 3 illustrates the simple band energy diagram for a biohybrid solar cell in a CSSC format, based on the above results. The agreement between the energy levels is the key factor for the functionality of the CSSC, since it provides the necessary driving force for the electron to jump through consecutive levels. We have, therefore provided a solid fundamental proof to show that this biohybrid equivalent of a DSSC is indeed viable, and that this device can be utilized for energy harvesting from a light source, particularly in using near-IR irradiation, which is relatively underutilized in conventional DSSCs.

As noted above, the recent development of an electrode utilizing chromatophores to generate light-dependent current in the presence of an external potential[7] raised the question of the function such applied voltages might play. Similar potentials have been utilized in the past to maintain quinone in an oxidized form[17] and it is possible that they facilitate electron cycling. Alternatively, such a potential might be required to give directionality to electron flow and to minimize charge recombination. Matching of the conductive band gaps in our CSSC provides a platform to directly test the latter explanation. Since electron flow is energetically favorable from TiO_2 to FTO, even an unmodified working electrode should be able to confer unidirectional movement of current. Indeed, this is what is observed with our CSSC device. When no “chromatophore dye” was present, the device was capable of generating a current (Fig. 1), but the current was significantly

reduced when 890-nm light was used instead (Fig. 2), since it lies beyond the absorbance by TiO_2. Moreover, RCs of *Rsp. rubrum* chromatophores excite electrons in a light-dependent fashion to levels above the conduction band of TiO_2, and when coupled to the TiO_2/FTO electrode, current is then carried from RCs to TiO_2 and ultimately to the FTO electrode. Quinone, which functions as primary electron acceptor in natural systems, has a midpoint potential of -200 mV during light-induced electron flow.[16] Since the midpoint potential of the conductive band of TiO_2 is -500 mV, the maximal voltage represents the difference between this value and the primary electron acceptor, or 300 mV. Indeed, during illumination with 890-nm light, the voltage measured was 0.29 V (Table 1). Also noteworthy are the efficiency measurements, which showed the highest value when chromatophores, and the biological electrolytes were irradiated with 890-nm light, surpassing even the efficiency of controls using white light.

This simple approach of replacing an organic dye with a natural photosynthetic membrane resulted in a functional CSSC that is capable of generating current using near-IR irradiation. A variation of this approach could extend the light harvesting capabilities of a tandem PSII-PSI system by replacing PSI with a near-IR photon absorbing LH1-RC core structure, resulting in increased solar conversion efficiencies and a better match of the solar spectrum to the electrochemical work.[2,18] Although the current generated in our system was not as high as that of the typical photovoltaic cells or DSSCs[1] when white light was used, it represents a highly viable approach for near-IR light utilization in which a natural system is replicated as a self-sustaining device in a synthetic manner. Further optimization is aimed at increasing both the long-term stability and quantum efficiency (now at ~0.04%) of this promising CSSC device.

METHODS SUMMARY

Wild-type *Rsp. rubrum* strain S1 was grown for ~3 d at a light intensity of 100 W/m^2 into mid-

logarithmic phase on a modified synthetic medium[19,20] in 1-L Roux bottles at 30°C. Chromatophores were isolated from French pressure cell extracts by rate-zone sedimentation on sucrose density gradients as described previously,[19] washed by ultracentrifugation and resuspended in 0.1 M Na_2PO_4 buffer (pH 7.2) at 29 mg protein/mL.

For fabrication of the chromatophore-sensitized solar cell (CSSC), we coupled chromatophores to mesoporous TiO_2 layer, following a procedure[15] in which 12 g of P25 TiO_2 particles (Evonik Degussa) were first ground in a porcelain mortar with 4 ml of deionized H_20 and 0.4 ml of acetylacetone. The viscous paste was slowly diluted with an additional 16 ml of deionized H_20 under continuous grinding and 0.2 ml of Triton X-100 was added to facilitate colloid spreading on the substrate. FTO-coated glass was used as the transparent conducting oxide substrate (15-30 Ω/cm^2, Hartford Glass). The coating of the photoanode from the TiO_2 paste was performed by doctor blading with Scotch tape defining the coating area, location, and thickness. The cell area defined by the TiO_2 film was 2 cm x 1 cm (2 cm^2), with film thickness varying from 10-12 μ. Film thickness and uniformity was measured by a profilometer (Tencor, Alpha-step 200). Films were dried in air for 1 h and sintered at 500°C for 1 h at a ramp rate of 5°C/min, followed by cooling at the same ramp rate. Heat treatment converted the TiO_2 to a100% anatase phase. The counter electrode consisted of a Pt layer, deposited by radio frequency sputtering for 2 min at100 W, producing a 200-nm thick film on the FTO. For fabricating the cell, the two electrodes were held together with binder clips, and separated by a Teflon spacer with a thickness of 40 μm, used as the medium for soaking the Q_0 and cytochrome *c* electrolytes.

References:

1. Lewis N. S. & Nocera D. G. Powering the planet: chemical challenges in solar energy utilization. *Proc. Natl. Acad. Sci. USA* **103,** 15729-15735 (2006).
2. McConnell I., Li, G. & Brudvig G. W. Energy conversion in natural and artificial photosynthesis. *Chem. Biol.* **17,** 434-447 (2010).
3. Badura, A. *et al.* Light driven water splitting for (bio-)hydrogen production: Photosystem 2 as the central part of a bioelectrochemical device. *Photochem. Photobiol.* **82,** 1385-1390 (2006).
4. Lubner, C. E. *et al.* Wiring an [FeFe]-hydrogenase with photosystem I for light-induced hydrogen production. *Biochemistry* **49,** 10264–10266 (2010).
5. Ciobanu, M. *et al.* Electrochemistry and photoelectrochemistry of photosystem I adsorbed on hydroxyl-terminated monolayers. *J. Electroanal. Chem.* **599,** 72-78 (2007).
6. Vittadello, M. *et al.* Photoelectron generation by photosystem II reaction centers tethered to gold surfaces. *ChemSusChem* **3,** 471-475 (2010).
7. Magis, G. *et al*. Light harvesting, energy transfer and electron cycling of a native photosynthetic membrane adhered onto a gold-surface. *Biochim. Biophys. Acta* **1798,** 637-645 (2010).
8. Lu, Y., Xu, J., Liu, B. & Kong, J. Photosynthetic reaction center functionalized nano-composite films: Effective strategies for probing and exploiting the photo-induced electron transfer of photosensitive membrane protein. *Biosens. Bioelectron.* **22,**1173-1185 (2007).
9. Trammell, S. A., Wang, L., Zullo, J. M., Shashidhar, R. & Lebedev, N. Oriented binding of photosynthetic reaction centers on gold using Ni-NTA self-assembled monolayers. *Biosens. Bioelectron.* **19,** 1649-1655 (2004).
10. Lebedev, N. *et al.* Conductive wiring of immobilized photosynthetic reaction center to

electrode by cytochrome *c*. *J. Am. Chem. Soc.* **128,**12044-12045 (2006).

11. Griva, I., Schnur, J. M. & Lebedev, N. The role of electrode curvature in controlling electron transfer between the photosynthetic reaction center protein and gold nanoelectrodes. *Chemphyschem* **11,** 3589-3591 (2010).
12. Suemori, Y. *et al.* Self-assembled monolayer of light-harvesting core complexes of photosynthetic bacteria on an amino-terminated ITO electrode. *Photosynth. Res.* **90,** 17-21 (2006).
13. O'Regan, B. & Grätzel, M. A low-cost, high-efficiency solar cell based on dye-sensitized colloidal TiO_2 films. *Nature* **353,** 737–740 (1991).
14. Parson W. W. & Warshel, A. in *The Purple Phototrophic Bacteria* (eds. Hunter, C. N., Daldal, F., Thurnauer, M. C. & Beatty, J. T.) 355–377 (Springer , Dordrecht, The Netherlands, 2009).
15. Nazeeruddin, M. K. et al., Conversion of light to electricity by cis-X2bis(2,2'- bipyridyl-4,4'- dicarboxylate)ruthenium(II) charge-transfer sensitizers (X = Cl-, Br-, l- , CN-, and SCN-) on nanocrystalline titanium dioxide electrodes. *J. Amer. Chem. Soc.* **115,** 6382-6390 (1993).
16. Timpmann, K., Zhang, F. G., Freiburg, A. & Sundström, V. Detrapping of excitation-energy from the reaction-center in the photosynthetic purple bacterium *Rhodospirillum rubrum.* *Biochim. Biophys. Acta* **1183,** 185-193 (1993).
17. Prince, R. C. & Dutton, P. L. The primary acceptor of bacterial photosynthesis: its operating midpoint potential? *Arch. Biochem. Biophys.* **172,** 329-334 (1976).
18. Blankenship, R. E. *et al.* Comparing potosynthetic and potovoltaic efficiencies and recognizing the potential for improvement. *Science* **332,** 805-809 (2011).

19. Inamine, G. S. & Niederman, R. A. Development and growth of photosynthetic membranes of *Rhodospirillum rubrum*. *J. Bacteriol*. **150,**1145-1153 (1982).

20. Ormerod, J. G., Ormerod, K. S. & Gest, H. Light-dependent utilization of organic compounds and photoproduction of molecular hydrogen by photosynthetic bacteria; relationships with nitrogen metabolism. *Arch. Biochem. Biophys.* **94,** 449-463 (1961).

21. Ahmed, S., Du Pasquier, A., Dunbar P., Birnie, D. P. & Asefa, T. Self-assembled TiO2 with increased photoelectron production, and improved conduction and tansfer: Enhancing photovoltaic performance of dye-sensitized solar cells. *ACS Appl. Mater. Interfaces* **3,** 3002–3010 (2011).

Supplementary Information is linked to the online version of the paper at www.nature.com/nature.

Acknowledgements This work was supported by the U. S. Department of Energy (Grant No. DE-FG02-08ER15957) from the Chemical Sciences, Geosciences and Biosciences Division, Office of Basic Energy Sciences, Office of Science (R.A.N.). T.A. gratefully acknowledges the financial assistance provided by the U. S. National Science Foundation through Grant Nos: CAREER CHE-1004218, NSF DMR-0968937, NSF NanoEHS-1134289, and the NSF- American Competitiveness and Innovation Fellowships (NSF-ACIF) for 2010 and the accompanying research grant and NSF Creativity Award in 2011.

Author Contributions K.W., S.A., A.V.B., T.A. and R.A.N. conceived the research. T.A, D.P.B. and R.A.N. supervised the research. S.A.. K.W., A.A.B, A.V.B and K.W. performed the experiments and analysed the data. K.W., S.A., T.A. and R.A.N contributed to the manuscript preparation.

Author Information Reprints and permissions information is available at www.nature.com/reprints. The authors declare that they have no competing financial interests. Readers are welcome to comment on the online version of this article at www.nature.com/nature. Correspondence and requests for materials should be addressed to K.W. (woronowicz@biology.rutgers.edu), or R.A.N. (rniederm@rci.rutgers.edu)

Table 1 **Solar J-V characteristics of solar cells under white light and 890-nm illumination**

Cell	I_{SC} (mA/cm^2)*	V_{OC} (V)†	*FF* (%)‡	η (%)§
TiO_2 (white light)	0.060	0.36	0.28	6.05×10^{-3}
TiO_2 (890-nm filter)	0.00122	0.16	0.00021	6.97×10^{-7}ξξ
TiO_2 + cytochrome *c* (white light)	0.040	0.32	0.26	3.33×10^{-3}
TiO_2 + cytochrome *c* (890-nm filter)	0.00193	0.07	0.67	1.54×10^{-3}ξξ
TiO_2 + Q_0 (white light)	0.0510	0.34	0.23	3.98×10^{-3}
TiO_2 + Q_0 (890-nm filter)	0.00194	0.13	0.53	2.27×10^{-3}ξξ
TiO_2 + Q_0 + cytochrome *c* (white light)	0.0230	0.25	0.23	1.33×10^{-3}
TiO_2 + Q_0 + cytochrome *c* (890-nm filter)	0.00680	0.12	0.21	2.91×10^{-3}ξξ
TiO_2 + chromatophores + Q_0+ cytochrome *c* (white light)	0.0528	0.33	0.25	4.36×10^{-3}
TiO_2 + chromatophores + Q_0 + cytochrome *c* (890-nm filter)	0.0247	0.30	0.29	3.66×10^{-2}ξξ

Photovoltaic I-V characterization was performed under AM 1.5 (100 mW cm^{-2}) illumination by a 300 W Xenon solar simulator.[21] The solar simulator and electrical characterization equipment were controlled by a labview program through which -1 to 1 V were fed to the solar cell with a step size of 10 mV.

*Short circuit current.

†Open circuit voltage.

‡Fill factor.

§Energy conversion efficiency.

ξξξNormalized to input power of 5.882 mW/cm.^{2}

Figure legends

Figure 1 Current-voltage curves of cells under white light and near-IR illumination. A. Solar behavior of cells under white light. The input power is 100 mW/cm^2, and the effective cell area is 0.25 cm^2. ISC, short circuit; VOC, open circuit voltage. B. Solar behavior of cells under 890-nm illumination. The input power was 5.88 mW/cm^2 and the effective cell area was 0.25 cm^2. Note that the TiO_2 only device does not exhibit a J-V curve and had an FF value ≈ 0 (Table 1), owing to absorption edge mismatch. See text for additional experimental details.

Figure 2 Dark Current behavior of cells. Forward bias provided is from -1 to +1 V with step size of 10 mV. Dark current trends show the following performance ranking in terms of least recombination: TiO_2 > TiO_2 + chromatophores + Q_0 + cytochrome *c* > TiO_2 + cytochrome *c* > TiO_2 + Q_0 >>TiO_2 + Q_0 + cytochrome *c*. This is essentially in accordance with J-V performance under white light (Table 1). When both Q_0 and cytochrome *c* were present, their effects were additive and recombination at the TiO2 electrode was the most affected. See text for additional experimental details.

Figure 3 Band energy diagram of biological dye sensitized solar cell. Oxidation-reduction potentials are presented in volts (V) vs. standard hydrogen electrode (SHE). Upon irradiation by light, electrons in the RC are raised from their ground state (S_0) to an excited state (S*), resulting in the initial charge separation. The energy level of the latter is above the conduction band edge of TiO_2, allowing the injection of the photoelectron into the TiO_2. The electron travels through an external circuit to perform useful work, and is reintroduced back into the cell through a Pt counter electrode. The Q_0 and cytochrome *c* potential (equivalent to redox electrolyte of a conventional DSSC) was slightly higher than the ground state of the chromatophores, and therefore the electron can be injected back into the RC to restore its original electronic configuration. It is important to

note that the Q_0 and cytochrome *c* potential was found using a back-calculation, where V_{OC} is the difference between TiO_2 conduction/Fermi level and the Q_0/cytochrome *c* potential. With the V_{OC} value obtained from the J-V measurements (~0.3 V), the actual potential of Q_0/cytochrome *c* could be determined. This potential is capable of producing the necessary driving force for the electron to jump through consecutive levels.

Supplementary Figure 1

Mercury porosimetry plot of incremental intrusion of mercury with respect to the pore diameter in the P25 TiO_2 film. Mercury porosimetry was performed with a Micromeritics Autopore 9400 porosimeter on the P25 TiO_2 film as previously described[21] by intruding mercury into the pores through application of pressure to the surrounding phase, which facilitated determination of porosity, pore size, volume and distribution. For sample preparation, a thick coating of titania dispersion was drop-cast and air dried for 2 h. This was followed by heating at 500°C for 30 min with a ramp rate of 2°C/min. Flakes of the coating were carefully collected to prevent disturbing internal microstructure. Prior to porosimetry, samples were dried at 200°C for 24 h. A single sharp pore peak is seen in the mesopore range at 29.4 nm. Total intrusion pore volume of the film was found to be 0.73 cm^3/g, with a film porosity of 56%.

Supplementary Figure 2

Field-emission scanning microscope (FESEM) images of the microstructure of the titania films examined on a model Zeiss Sigma FESEM. For obtaining these images, the samples were coated with iridium using a Gatan Model 681 Ion Beam Coater to prevent charging effects. A. Buffer (0.1 M Na_2PO_4 pH 7.2); B. Chromatophores in buffer. In

circled region, chromatophores are seen partially inserted into the pores or sitting at the surface.

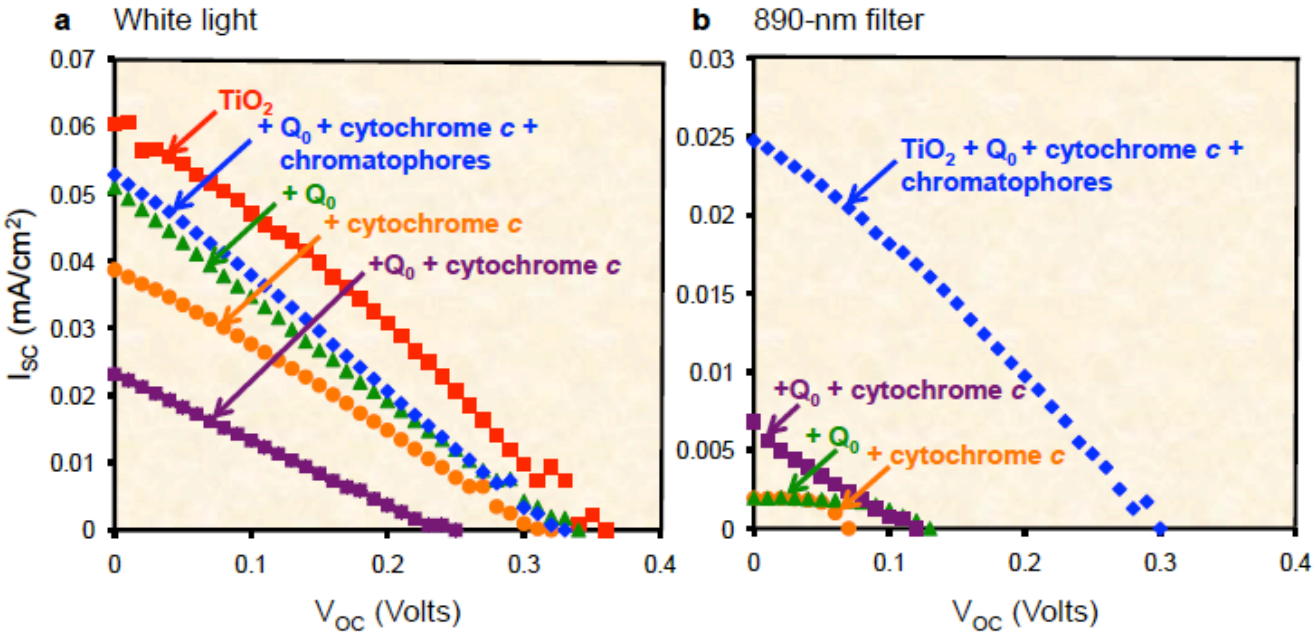

Figure 1

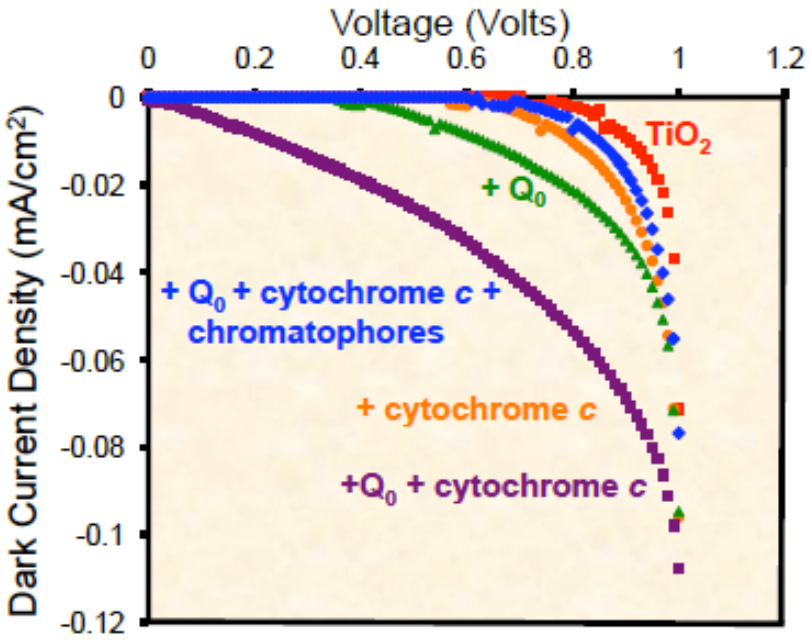

Figure 2

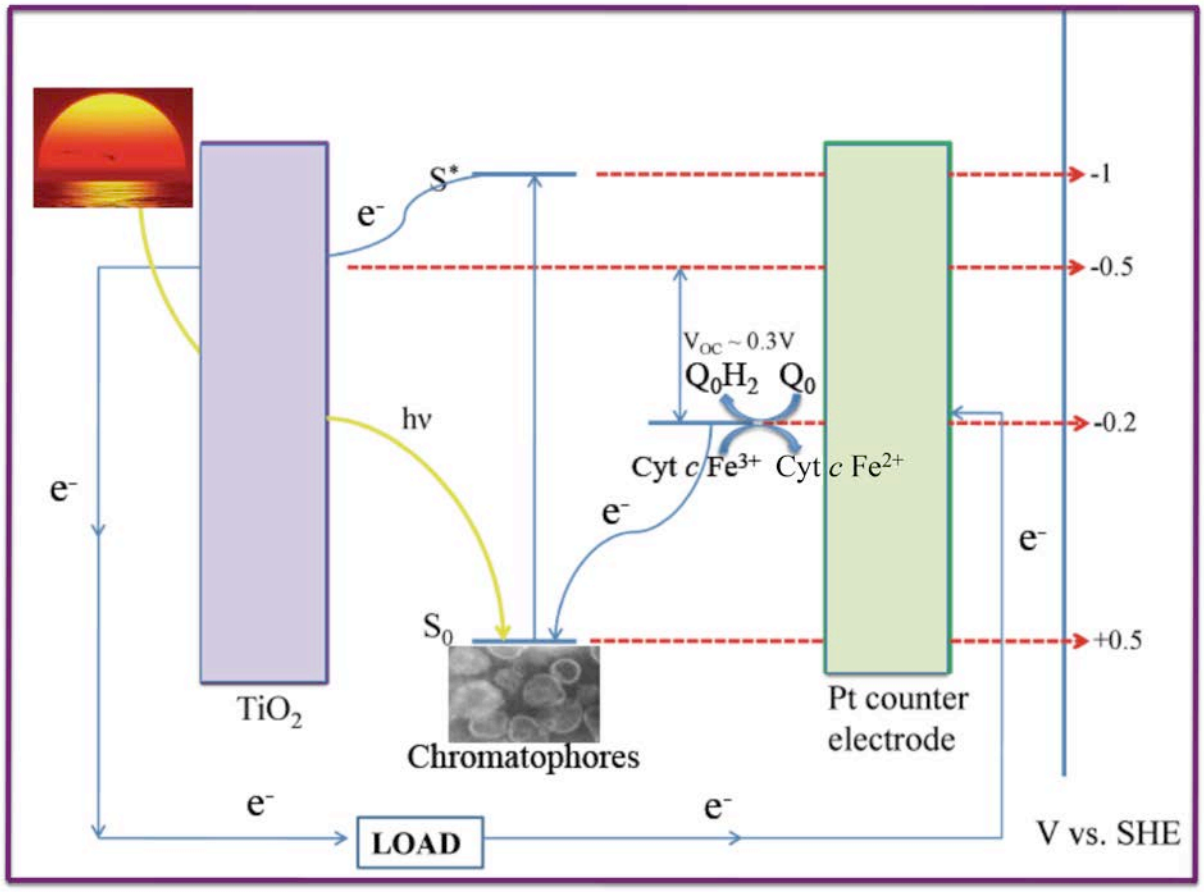
S*
e⁻
-1
-0.5
V_{OC} ~ 0.3V
Q_0H_2 Q_0
hν
-0.2
Cyt *c* Fe^{3+} Cyt *c* Fe^{2+}
e⁻
e⁻
e⁻
S_0
+0.5
TiO_2
Chromatophores
Pt counter electrode
e⁻
e⁻
LOAD
V vs. SHE

Figure 3

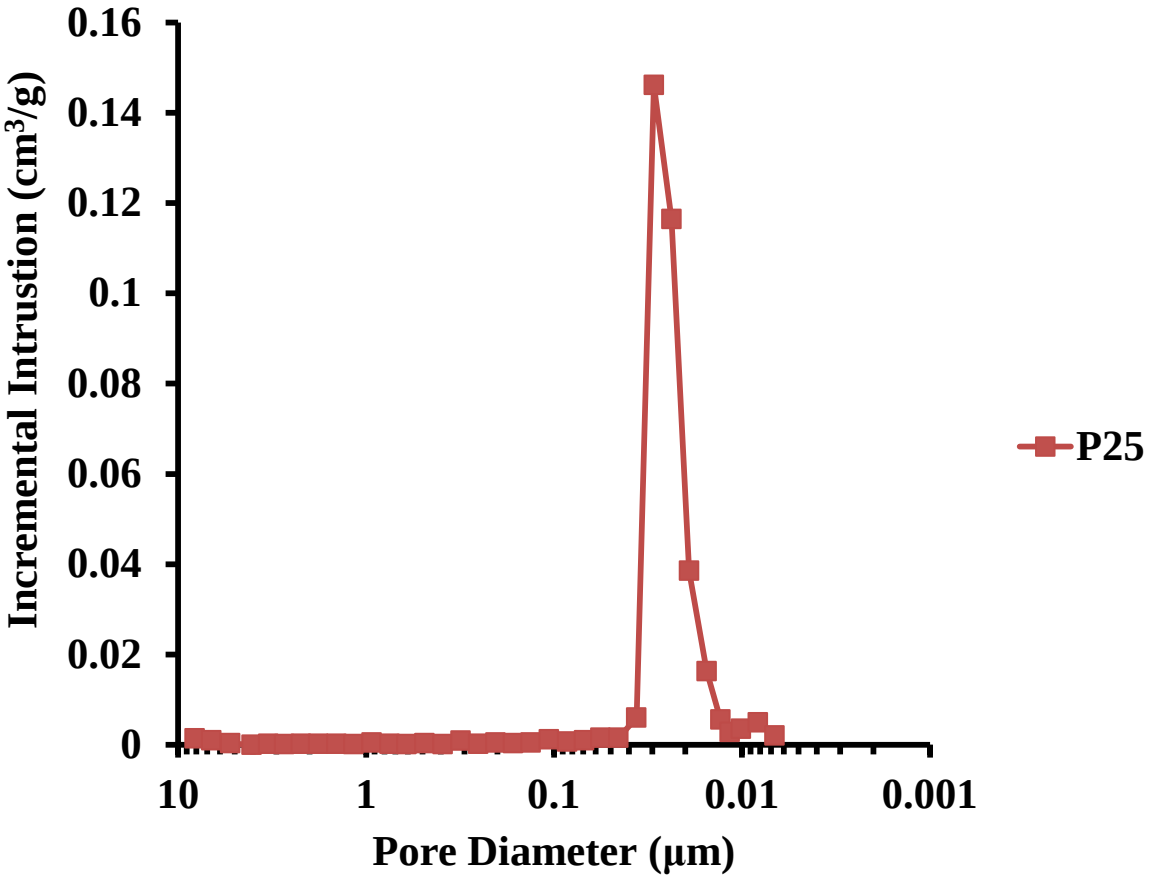

Supplementary Figure 1

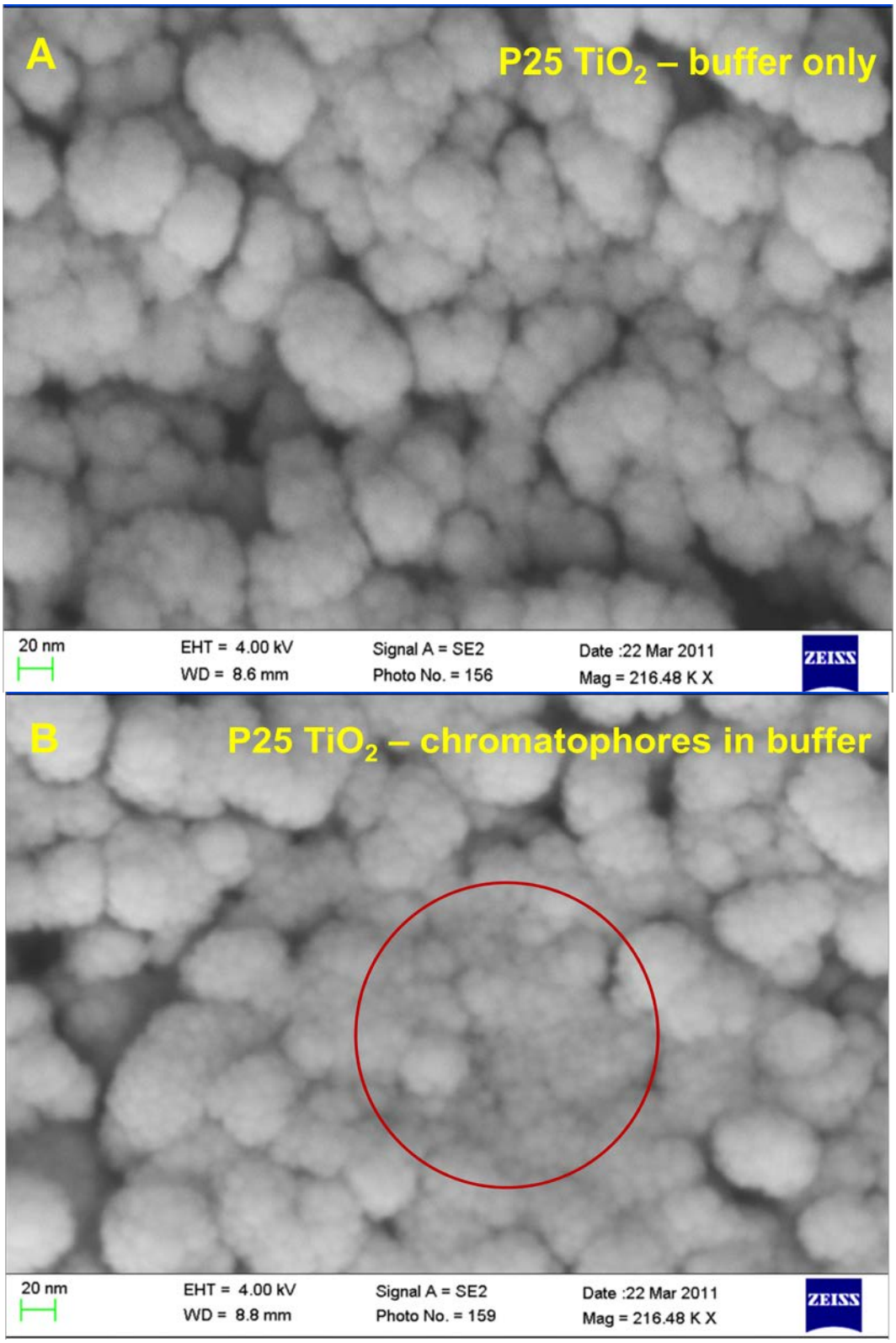

Supplementary Figure 2